Bringing light to galaxy formation simulations[1]

Sergio Gelato
SISSA, 2–4 via Beirut, I–34013 Trieste, Italy

Fabio Governato
Department of Astronomy, FM–20, University of Washington, Seattle WA 98195, USA

ABSTRACT

Models of galaxy formation ultimately aim at reproducing the *observed* properties of galaxies. We report on work in progress to predict luminosities, colours and morphologies of field objects of various masses through N-body + SPH simulations. We describe our method, illustrate the effects of varying the star formation assumptions, show some preliminary results, draw encouragement from their strengths as well as lessons about what improvements are most needed.

1. Introduction

N-body simulations are a well established tool to test theories of structure formation in cosmology. Within their domain of validity—whenever gravity is the single dominant physical process, as may be the case on sufficiently large scales for a universe dominated by cold dark matter (CDM)—they yield robust predictions about the numbers, size distribution and clustering properties of mass condensations in any given cosmological model. Their potential for new useful discoveries is not yet exhausted, as the recent work of Navarro et al (1996, hereafter NFW) illustrates.

Unfortunately their predictions about the *mass* distribution don't easily lend themselves to a comparison with observations, which only detect *radiation* sources. It is now very clear that on scales as small as individual galaxies the light is a poor tracer of the mass. Connecting the two requires further modelling, whether one adopts the "inverse" approach of deducing the mass distribution from the properties of the luminous material or the more "direct" one of adding to the N-body simulations the main physical (thermodynamical, chemical, nuclear) processes that "give light" to galaxies. In both cases we are faced with huge uncertainties stemming from our lack of understanding of the key processes of star formation and feedback to the interstellar medium. The inverse approach has the additional drawback of discarding some observational information; this becomes increasingly wasteful as the quality and quantity of observations improves. At the

[1]Slightly expanded version of article to appear in *Dark and visible matter in galaxies*, editors M. Persic and P. Salucci, ASP Conference Series.

same time, advances in computing power and in numerical techniques are making direct simulation ever more practical. The pioneering work of Katz (1992), Navarro & White (1993, hereafter NW), Steinmetz & Müller (1995), to cite but a few, serves as a springboard for further exploration of this area of crucial interest for cosmology.

To predict galaxy luminosities and spectra, we must keep track at the very least of the cooling and condensation of primordial gas, of the formation and evolution of stars, of the stars' feedback on the state and composition of the surrounding gas. Our ignorance of the details of these processes, and Occam's razor, call for very schematic models with few free parameters, based mainly on simple conservation laws. We assume that star formation occurs predominantly in cold, high density, collapsing gas and that the energy of supernova winds eventually heats the surrounding gas. A test bed for these "recipes" is provided by the recent wave of semi-analytic models of galaxy formation (reviewed by Frenk at this conference). We can also draw useful lessons from a line of research (exemplified by Pardi et al 1995) that relies on very detailed chemical evolution models to deconvolve the formation history of observed stellar populations in the Milky Way. While valuable as sources of observational constraints and analysis techniques, such models don't readily help us choose among cosmological scenarios. And like the semi-analytic models, they treat only schematically the spatial dependence of the star formation and feedback processes, the explicit inclusion of which is one of the N-body method's greatest strengths.

This method is still in its infancy, which means we must learn more about the validity of our model assumptions before we can draw firm conclusions about which cosmogony is the correct one for our universe. But in the long run we hope and expect direct simulations to shed light over many outstanding questions, such as: the origin of the morphology-density relation; the overabundance of dwarf galaxy halos in CDM; the relation between total galaxy mass and the shape of the rotation curve; the nature of the faint blue galaxies; the "nature vs. nurture" hypothesis for the origin of elliptical galaxies; the origin of low surface brightness galaxies.

2. The method

2.1. Initial conditions

We start with a Gaussian random field with an $\Omega = 1$ cold dark matter (CDM) power spectrum normalized to $\sigma_8 = 0.7$ at the present epoch on a periodic three-dimensional grid of 256 nodes and 32 Mpc on a side. We adopt $H_0 = 50\,\mathrm{km\,s^{-1}\,Mpc^{-1}}$, so that σ_8^2 is the mass variance within a sphere of radius 16 Mpc. This choice of parameters may not yield the best fit to observations, but it is a standard benchmark for this class of simulations.

The density field is first evolved using a particle-mesh code, and interesting halos, defined as connected high density ($\delta\rho/\rho > 57$) regions, are selected from the final state. In this report we present results for two halos, code-named B6 and B9, with respective circular velocities V_c

of 260 and 120 km s^{-1}. These halos were chosen to lie outside clusters, and are thus expected to correspond to spiral rather than elliptical galaxies. The initial location of each halo is then resampled with equal numbers of gas and dark matter particles (3000 to 4000 each) in a sphere large enough to hold the protohalo. Surrounding concentric spheres are sampled with collisionless particles only, at progressively coarser resolution, to produce a realistic tidal field. The particle positions and growing-mode velocities are obtained by perturbing a 128^3 (B6) or 256^3 (B9) lattice according to the Gaussian random field realization mentioned earlier, which already includes all the short-wavelength power we need.

2.2. SPH simulations

Smoothed Particle Hydrodynamics (SPH) is reviewed in Monaghan (1992). Our implementation is an evolution of that of NW. The most significant additions are: a heat source that mimics a photoionizing UV background (Navarro & Steinmetz 1996); a few alternative star formation recipes; bookkeeping of the mass of heavy elements produced in stars and returned to the gas.

The gravitational softening, 1.25 kpc (B9) to 2 kpc (B6) for the gas and twice as much for the DM, allows us to start the simulations at $z = 39$ and $z = 29$ respectively. Our minimum time step, dictated by accuracy and stability requirements, is about 2×10^5 yr, making a complete simulation rather time consuming.

The cooling function incorporates Bremsstrahlung and atomic line cooling for a primordial Mixture of H and He, but no H_2 cooling. For the time being we also neglect the enhancement to the Bremsstrahlung as heavy elements are added to the gas.

In some runs we include a heating term from an ultraviolet photon background, such as might be produced by quasars and Population III stars. This background modifies the ionization equilibrium of the gas, particularly at low densities, reducing the cooling rate as well as providing additional energy. We follow existing practice by choosing a flux

$$J_\nu(z) = J_{-21}(z) \times 10^{-21} \left(\frac{\nu_L}{\nu}\right)^\alpha \,\mathrm{erg\,s^{-1}\,cm^{-2}\,sr^{-1}\,Hz^{-1}} \tag{1}$$

with $\alpha = 1$ (more appropriate[2] to a non-stellar origin of the photons) and

$$J_{-21}(z) = \frac{1 - e^{z-8}}{1 + [5/(1+z)]^4} \tag{2}$$

for $0 \le z \le 8$. Our normalization agrees well with observational determinations of the UV flux (Giallongo et al 1996).

[2]Perhaps even a little too hard, given a mean quasar spectral index $\alpha \sim 1.5$ and the presence of intervening Ly α absorbers. We merely followed the example of Katz et al (1996) and Navarro & Steinmetz (1996). Given the crudeness of other aspects of our method, this discrepancy should be no particular cause for concern.

We allow stars to form in regions where the gas flow is convergent and the gas density exceeds $7 \times 10^{-26}\,\mathrm{g\,cm^{-3}}$. A similar value of $1.67 \times 10^{-25}\,\mathrm{g\,cm^{-3}}$ has been advocated by Kennicut (1989) on observational grounds. This threshold guarantees that the gas can cool to 10^4 K in much less than the local dynamical time $t_d = (16G\rho/3\pi)^{-1/2}$, contracting isothermally afterwards. Where these prerequisites are satisfied, the gas is turned into stars at a rate $d\rho_{\mathrm{gas}}/dt = -\rho_{\mathrm{gas}}/t_d$. We discretize the process by waiting a time $t_d|\ln(1-\varepsilon)|$ before turning a fraction ε of an eligible gas particle into a new particle of coeval stars; our conditions for star formation must remain satisfied throughout this finite time interval. The value of ε sets our time resolution of the star formation event. In this particular set of simulations we found adequate convergence for $\varepsilon \lesssim 0.15$.

For comparison, we tried raising the density threshold, either explicitly to the Kennicut value or by requiring that the gas be Jeans unstable on the smallest resolved scale: $t_s \equiv h/c_s > t_d$, where $c_s \sim 12\,\mathrm{km\,s^{-1}}$ is the sound speed and h the local gas resolution (taken as the greater of the SPH smoothing and gravitational softening lengths). This amounts to a resolution-dependent density threshold $\rho > m^{-2}(3\pi c_s^2/16G)^3$, where m is the mass of a gas resolution element. Such behaviour can be useful to counteract the effect that lower resolution implies averaging of the density over larger regions. In our B9 runs the implied threshold is higher than Kennicut's.

Once formed, a star particle begins to lose mass to the surrounding gas particles at every integration step according to standard stellar evolution models. (For this and other purposes we assume a Salpeter IMF between 0.1 and 40 $M_\odot$.) Thermal energy is dumped into the gas as part of the same process. Pending further tests, we do not add bulk kinetic energy to the gas.

We keep track of the mass in elements heavier than Helium ("metals"). This is initially zero for all gas particles, and stars inherit the metal fraction of their parent gas particles. The material they feed back to the gas contains this same fraction, enriched by the mass newly produced in supernova progenitors according to the following fit to Woosley and Weaver's (1995) data:

$$M_Z(M) = 2.935 - 0.65M + 4.59 \times 10^{-2}M^2 - 6.57 \times 10^{-4}M^3 \tag{3}$$

(M_Z and M in solar masses). We shall express our results for $Z \equiv M_Z/M$ in terms of the solar metallicity $Z_\odot = 0.02$.

2.3. Stellar population synthesis

Each star particle ($\sim 10^6\,M_\odot$) created during a run can be regarded as a simple stellar population (SSP), i.e. a set of coeval stars of uniform metallicity and known mass function. We synthesize maps and spectra for a simulated galaxy by summing the spectral energy distributions (SEDs) tabulated for SSPs by Bruzual & Charlot (1993), and so trace the magnitude and colour evolution of the object.

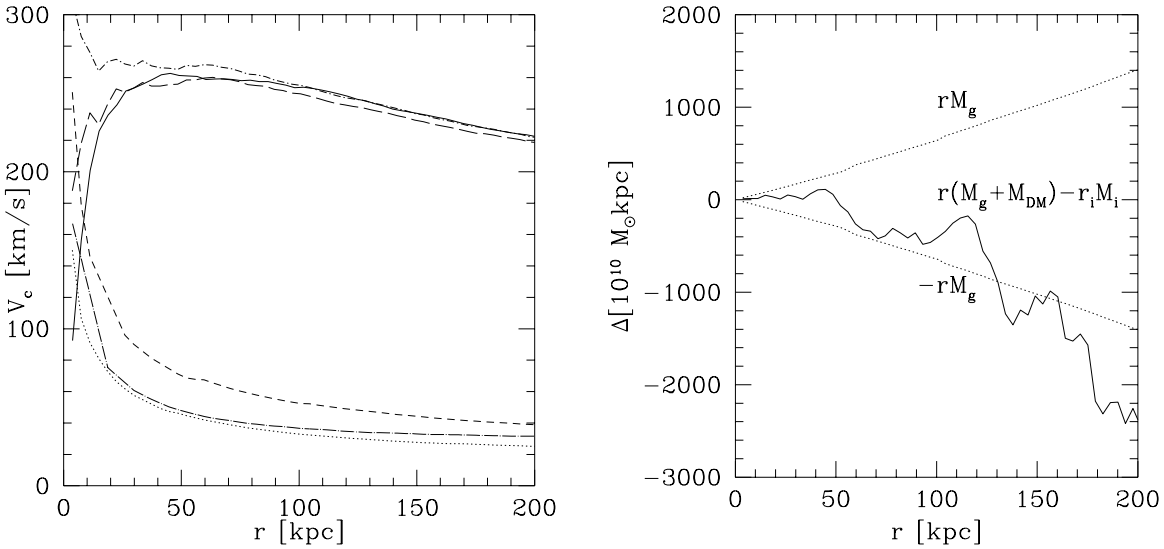

Fig. 1.— *Left:* rotation curve $V_c(r) \equiv GM(< r)/r$ at $z = 0$ for runs with dark matter only (full curve), $\Omega_b = 0.05$ (dark matter, long dashes; gas, short dashes; total, dot-short dash), $\Omega_b = 0.025$ (gas, dotted curve), and $\Omega_b = 0.05$ with UV heating (gas dot-long dash curve). *Right:* demonstration of the adiabatic invariance of $rM(< r)$ by comparing the radial profiles wirh dark matter only ($r_i M_i$) and with $\Omega_b = 0.05$ ($r(M_{\rm DM} + M_{\rm gas})$). At $r \lesssim$ 50–100 kpc, the difference $r(M_{\rm DM} + M_{\rm gas}) - r_i M_i$ (solid curve) is small by comparison with $rM_{\rm gas}$ (dotted curves).

3. Runs and results

3.1. Runs without star formation

For both our halos, we first perform a simulation with only dark matter particles. We compare these results to those of runs with cooling gas but no star formation (with baryon fractions $\Omega_b = 0.05$ and 0.025; the latter is expected to cool about twice as slowly by virtue of the lower gas densities).

At $\Omega_b = 0.05$ most of the gas within the virial radius condenses at the centre, forming a disk of radius comparable to the gravitational softening and causing the total rotation curve to rise more than would be consistent with observations. This cooling catastrophe is reduced by halving Ω_b, as expected. Introducing a UV heating term has a similar effect at large radii, but in addition suppresses the outer part of the central disk. Confirming previous works, these results suggest that some form of heating due to star formation is needed to form systems with a distribution of baryons similar to that of observed spiral galaxies. The left panel of figure 1 compares rotation curves for the gas component from these various runs.

The collapsing gas pulls along some of the dark matter, causing the halo to become more centrally concentrated. Previous studies (e.g., NFW) have relied on the adiabatic invariance of $rM(< r)$ (Gunn 1977) to estimate this effect. We tested this assumption by comparing the profiles

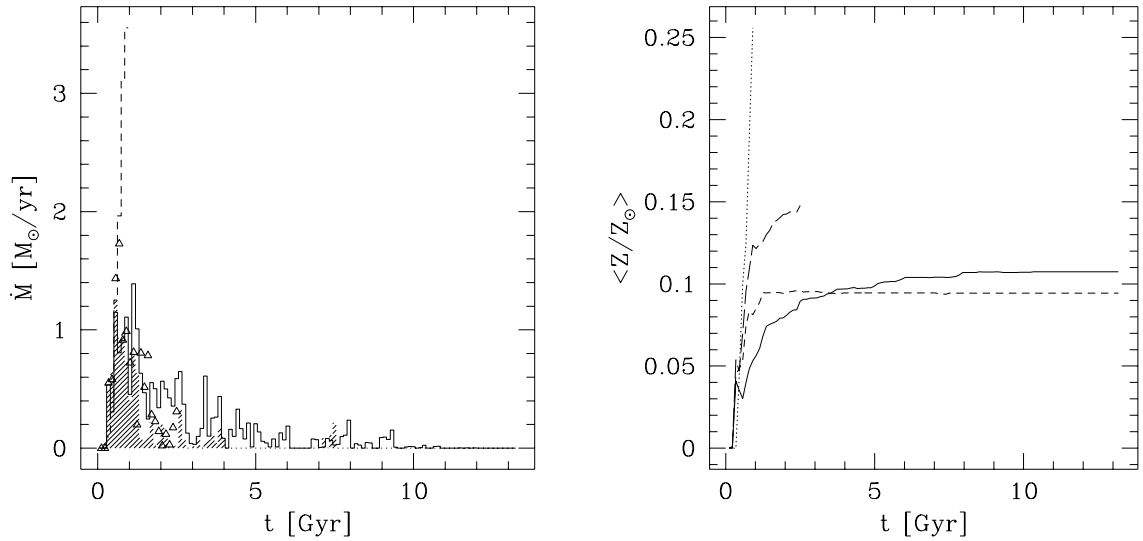

Fig. 2.— *Left:* Star formation rate as a function of time since the start of the simulation ($z = 39$), for $V_c = 120\,\mathrm{km\,s^{-1}}$. Solid curve: no heating. All others include UV heating. Shaded histogram: same star formation recipe. Triangles: higher density threshold. Dashed curve: $t_s > t_d$ requirement included. *Right:* Cumulative mean metallicity of the stars in that same halo. Solid curve: standard star formation recipe, no UV. Dashes: same recipe, with UV. Long dashes: higher density threshold. Dotted curve: $t_s > t_d$.

for our DM-only and cooling gas runs, and found that it holds: at small radii ($r \lesssim 50$ kpc), where the adiabaticity condition that the dynamical time be much shorter than the gas infall time is satisfied, the difference between the rM profiles is much smaller than the smallest individual term ($rM_{\rm gas}$) in the comparison. This is illustrated by the right-hand panel of figure 1.

3.2. Runs with star formation

For each halo we performed two sets of runs using our fiducial star formation recipe, one with and the other without UV heating. We also tested alternative recipes on the small halo. Figure 2(left) shows the star formation rates for the smaller halo. The ones for the other halo are an order of magnitude larger (10 vs. 1 $M_\odot\,\mathrm{yr}^{-1}$), and exhibit the same decay with a time scale of ~ 3 Gyr after the initial burst. The rates are in the observed range for high-z galaxies (Steidel et al 1996). Star formation almost ceases when $z \lesssim 0.5$. The UV background further suppresses star formation at late times, but is not nearly as effective in the early phases when the density is still high.

Raising the density threshold causes only a modest increase in the star formation rate, showing that our results are not critically sensitive to the exact value used. A higher density threshold means

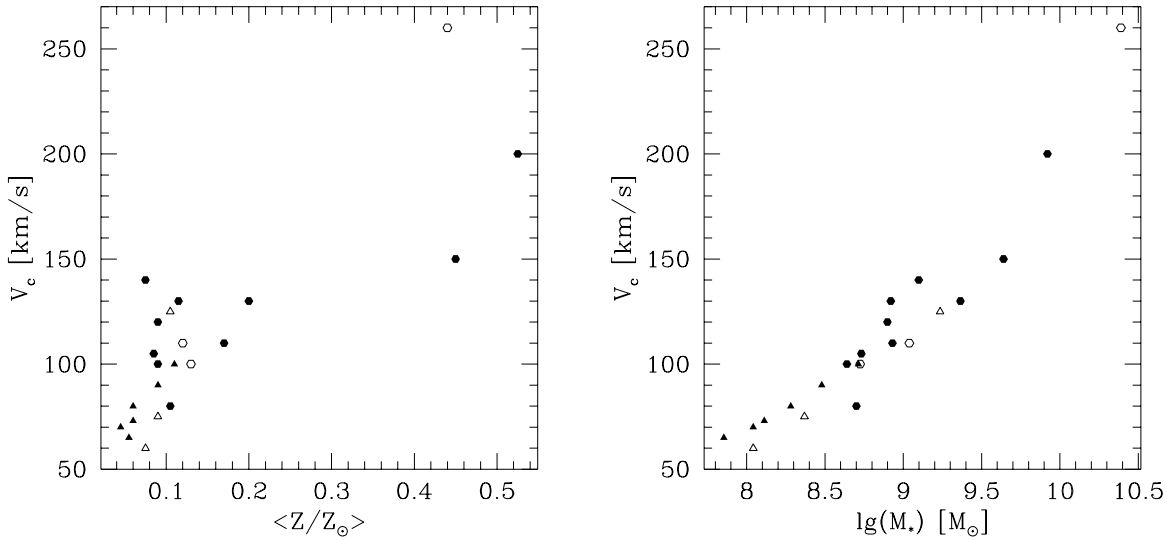

Fig. 3.— Correlation between circular velocity V_c and mean metallicity (left) and mass in stars (right) for various sub-halos at $z \sim 2$ (filled symbols) and $z \sim 0.5$ (open symbols). Hexagons are from our larger B6 simulation, triangles from the smaller, higher resolution B9 run.

that the supernova feedback will reheat the gas to a lower temperature, allowing it to cool again more quickly; this leads to greater recycling of the gas, which will also be visible in the metallicity evolution. Imposing the Jeans instability criterion (dashed curve) results in a spectacular increase in the star formation rate. Our feedback is clearly too weak to prevent runaway burning of all the available gas in this case.

Metallicity turns out to be a powerful discriminant between star formation models. Figure 2(right) shows the mean metal content of all stars formed up to a given time; the curves become horizontal when star formation stops. (Results for the larger halo are $Z/Z_\odot \sim 0.3$–0.4.) The UV background causes the metallicity to rise faster at first, since the star formation is restricted to higher densities where the feedback is less effective at mixing the material; but overall the longer duration of the star formation phase without UV heating leads to slightly higher metal fractions. Raising the density threshold produces a moderate increase in the metallicity, while the Jeans instability criterion has more spectacular consequences, leading to uncomfortably high mean Z values for a small galaxy at high redshift.

By $z = 0$ our objects have "puffed up" and acquired a very extended envelope where old, metal-poor stars from accreted lumps dominate the gas out to 150–200 kpc. These might correspond to the dwarf spheroidal satellites of galaxies like the Milky Way, but the resolution of our simulations does not allow a firm identification.

It can be useful to study the individual lumps before they merge. Figure 3 shows a tight Tully-Fisher-like correlation between the mass in stars and the circular velocity, and a weaker but

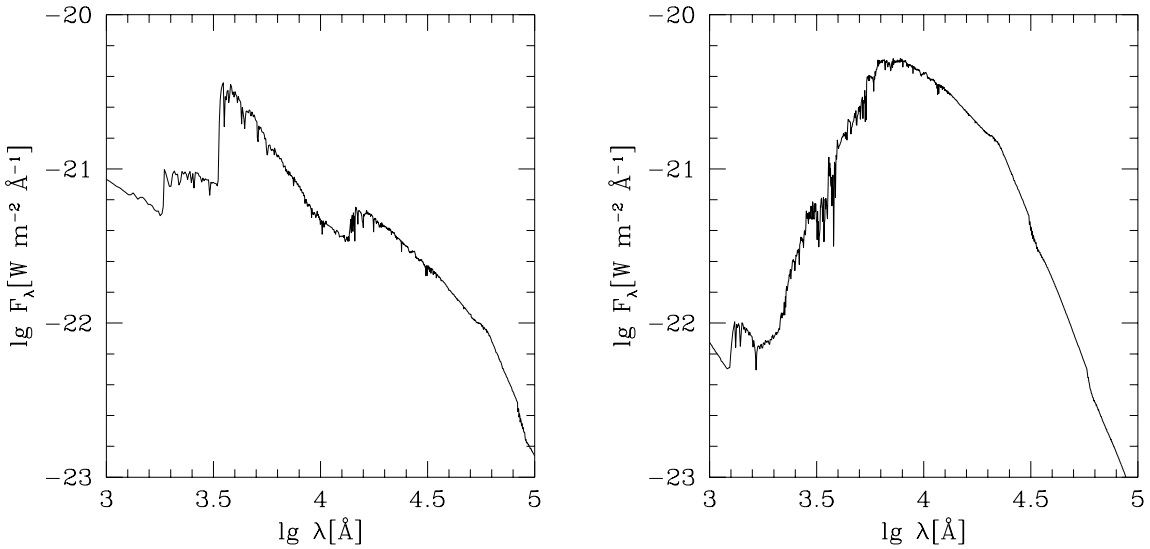

Fig. 4.— Spectral energy distribution for the $V_c = 120$ km/s halo at $z = 2.64$ (left) and at $z = 0.36$ (right). The abscissa is wavelength in the observer's frame, the ordinate the flux per wavelength interval. We assumed $\Omega = 1$, $H_0 = 50$ km/s/Mpc.

still clear link between circular velocity and mean metal enrichment. The correlations show little evolution between $z \sim 2$ and $z \sim 0.5$, although naturally the mean V_c does increase. That data from both our simulations, with different mass resolutions, fit essentially the same curve gives us some confidence that these particular trends are not too sensitive to the details of our method. Unfortunately, while the trend is qualitatively right, the slope of the relation between the mass in stars and the circular velocity is shallower than in the fits of Persic et al. (1996). Thus we have not yet solved the well-known problem of forming too many stars early on in small halos. This will probably require a better understanding of what triggers star formation in primordial gas. It has also been suggested (White & Frenk 1991) that a stronger supernova feedback may help cure this problem; we plan to investigate this idea in more detail.

Finally, we present in figure 4 the SED for our B9 halo (fiducial recipe, with UV) at $z = 2.64$ (left) and $z = 0.36$ (right), synthesized with Bruzual & Charlot's (1996) library which takes account of the ages and metallicities of the individual SSPs. The results have been translated into wavelengths and fluxes in the observer's frame, but we haven't yet accounted for IGM absorption (Madau 1995). These two redshifts correspond respectively to a starburst phase and to a time at which star formation has long since ceased.

4. Discussion

Some significant aspects of our simulation results are in good agreement with observations. The star formation peaks in a reasonable redshift range $2 \lesssim z \lesssim 3$. A related success is that the SEDs of the simulated galaxies at these redshifts look much like those of observed objects. Expected trends such as the relation between halo mass and star formation rate, or between halo mass and metallicity, are reproduced at least qualitatively, and we hope that the remarkable tightness of the correlations will lead to a strong calibration of the star formation prescription. Such calibration is a necessary task, since plausible variants of the prescription yield very different outcomes. This is both a curse (it decreases our confidence in the more quantitative aspects of the results) and a blessing, or at least a promise that something useful may be learned about the star formation and feedback processes.

The results at low redshift are less satisfactory. The fact that we cannot sustain star formation to $z = 0$ in objects that we'd like to identify with spiral galaxies is a disappointment. It could signal a flaw in the star formation algorithm. It could also be due in part to our limited resolution, which favours the formation of a hot, diffuse gas phase and may underestimate the amount of cool gas available at late times to form a rotationally supported disk of the appropriate size and mass. Convergence studies will clearly be important in settling this issue. In particular the dependence of the star formation and feedback recipes on the numerical resolution deserves close attention.

The current description of the feedback is probably inadequate: without incorporating some form of kinetic energy injection, the heating is too weak to prevent runaway star formation when the gas density is high, which will happen more easily in higher resolution models. As noted by NW (and confirmed by our own tests) the results are very sensitive to the (arbitrary) magnitude of this kinetic energy injection. It would be useful to lift this arbitrariness with the help of studies of the propagation of supernova winds in the ISM.

A difficulty should be noted in our implementation of the metallicity evolution: we did not account for dilution of the heavy element abundances by mixing in the ISM. Consequently, we may be overestimating the scatter in stellar metallicities, and in some models (with a high $\rho_{\rm min}$ and weak feedback) the mean metallicity as well.

It appears from a scan of recent literature that the art of modelling the cooling of gas within dark matter halos is approaching maturity, with convergence properties and spurious heating effects being addressed. Including star formation is the next step, and much progress is still needed before we can have full confidence in our models' predictions. Our preliminary results, uncertain as they may be, show some encouraging similarities with observational data. They also exhibit some rather tight relationships that should be eminently testable; this last fact is reason enough to continue perfecting this simulation technique.

We thank Julio Navarro for kindly making his SPH code available to us, and Adriano Fontana,

George Lake, Julio Navarro, Massimo Persic, Tom Quinn, Paolo Salucci for stimulating discussions.

REFERENCES

Bruzual, G., & Charlot, S. 1993, ApJ, 405, 538

Giallongo, E., Cristiani, S., D'Odorico, S., Fontana, A., & Savaglio, S. 1996, ApJ, 466, 46

Gunn, J. E. 1977, ApJ, 218, 592

Katz, N. 1992, ApJ, 391, 502

Katz, N., Weinberg, D. H., & Hernquist, L. 1996, ApJS, 105, 19

Kennicut, R. 1989, ApJ, 344, 685

Madau, P. 1995, ApJ, 441, 18

Monaghan, J. J. 1992, ARA&A, 30, 543

Navarro, J. F., Frenk, C. S., & White, S. D. M. 1996, ApJ, 462, 563 (NFW)

Navarro, J. F., & Steinmetz, M. 1996, preprint astro-ph/9605043

Navarro, J. F., & White, S. D. M. 1993, MNRAS, 265, 271 (NW)

Pardi, M. C., Ferrini, F., & Matteucci, F. 1995, ApJ, 444, 207

Persic, M., Salucci, P., & Stel, F. 1996, MNRAS, 281, 27

Steidel, C. C., Giavalisco, M., Pettini, M., Dickinson, M., & Adelberger, K. L. 1996, ApJ, 462, L17

Steinmetz, M., & Müller, E. 1995, MNRAS, 276, 549

Weinberg, D. H., Hernquist, L., & Katz, N. 1996, preprint astro-ph/9604175

White, S. D. M., & Frenk, C. S. 1991, ApJ, 379, 52

Woosley, S. E., & Weaver, T. A. 1995, ApJS, 101, 181